EFFECT OF PROPPANT TRANSPORT ON HYDRAULIC FRACTURE GEOMETRY

By

Michael W. Conway,
STIM-LAB, Inc.

Robert D. Barree,
Marathon Company

Abstract

Slurry transport and settling experiments were conducted to improve current descriptions of proppant transport. Results of these experiments were used to formulate a new slurry transport model which was incorporated in a fully three-dimensional fracture simulator. The model was tested and verified against experimental observations of slurry transport in a 4 foot by 16 foot slot model. Results of the study indicate that proppant slurry transport can be accurately modeled when the effects of single particle settling, density driven flow, particle velocity profiles, and slurry rheology are accounted for.

When the generation of fracture geometry is fully coupled with slurry transport, major alterations in the predicted final propped fracture are observed. Examples are provided to demonstrate the importance of proppant scheduling in controlling the final placement of proppant in hydraulic fractures.

Introduction

It has been a long-sought goal in hydraulic fracturing technology to accurately predict proppant slurry transport in non-Newtonian fluids. Numerous references exist in the petroleum literature describing various aspects of particle and slurry transport.

In the earliest studies relating to hydraulic fracturing applications, Kern and Perkins[1] investigated sand transport in low viscosity fluids. They concluded that transport relies on high frontal velocity of the fluid and that rapid sedimentation of sand creates an immobile "dune" along the bottom of the fracture which restricts the fracture height open to flow. This leads to high local fluid velocities and establishment of an equilibrium sand bed height.

Other authors[2-4] reported observing significant settling and less than perfect transport in both horizontal and vertical fractures. These studies, conducted in 1965-67, included the effects of particle size, drag coefficient, density, velocity, viscosity, and fluid yield point. The authors concluded that settling and particle segregation occur even in horizontal fractures and that the dense slurry accumulated on the bottom of the crack remains mobile but has a lower velocity than the average fluid speed.

In 1977, Novotny reported results of proppant transport studies conducted with non-Newtonian fluids. These observations showed that particles occupy different positions across the width of a vertical fracture at various shear rates and solids loadings.[5] He also reported that particle settling rate is strongly influenced by fluid shear rate and the presence of the fracture walls.

In the same year Clark, *et al.*, used a large scale slot flow model similar to that employed in this study to investigate proppant settling velocities after shut-in.[6] These studies concluded that particle clustering can result in an increased settling velocity. The results presented were preliminary and did not address bulk slurry movement.

At about the same time Hannah, Harrington, and others utilized a cylindrical flow cell to study single particle settling rates in non-Newtonian fluids while under representative shear.[7-8] They concluded that Stokes' Law can be applied, but may need to be modified by inclusion of an additional term to account for crosslinked fluid behavior.

These conclusions were partially supported by later work which indicated that single particle settling in crosslinked fluid depends on more complex parameters than just fluid viscosity.[9-10] However, these authors expressed some doubt whether Stokes' Law could be applied at all for these fluid systems.

Other authors reported studies of particle settling and transport in non-Newtonian crosslinked fluids.[11-14] These authors variously concluded that particle clustering does increase the observed settling rate and that bulk average viscosity of the fluid does not adequately describe settling velocity for a single particle. Wall effects and low shear viscosity were suggested as important considerations in predicting settling velocities. Differences between observed particle velocities and bulk fluid velocities in lateral flow were also noted.

Roodhart provided additional evidence of the importance of low shear, or "zero shear" viscosity on observed settling rates in non-Newtonian fluids.[15] He also observed that settling rate varies across the width of the fracture channel, depending on local shear conditions. Other authors reported results of particle settling experiments in viscoelastic fluids.[16-19] Their results suggest that viscoelasticity increases the dynamic settling rate at intermediate shear rates, but has little effect at low shear.

Clifton and Wang assimilated most of the theories available at that time in a multi-dimensional numerical model of proppant transport.[20] This model included the effects of particle-fluid slip velocity but ignored the effects of particle position within the slot. Unfortunately this model, like all previous references, relied solely on single particle settling equations such as Stokes' Law with modifications for particle hindering, wall effects, and various other factors. The effects of fluid bulk density gradients on the overall fluid potential distribution were not considered.

In areas outside the fracturing literature, especially in fluid mechanics, sedimentation, and waste disposal, the importance of bulk density gradients, or gravity induced flows, have been considered.[21-23] The effects of density currents on vertical and inclined flow have been modeled for systems of vapors, liquids, and suspensions of small particles. It has been shown that suspensions of solid particles can be modeled as a bulk phase when the single particle settling rate is small.[23]

The principal emphasis of the fracture design study described in this report was to examine the role of proppant scheduling on fracture geometry and final proppant placement. The fully 3-D simulator used in this study was developed by Marathon and the characteristics of the Grid Oriented Hydraulic Fracture Extension Replicator (GOHFER) have previously been described.[24] More recently, the performance of GOHFER was compared to other simulators in a GRI supported hydraulic fracture simulation study.[25] This work was made possible by the development of an improved numerical model of proppant transport. The model has been described in detail and will only be summarized here.[26]

Summary of Numerical Proppant Transport Simulator Characteristics

Proppant Velocity: It is well known that fluids flowing in a channel in laminar flow will have zero forward velocity at the channel wall, and reach a maximum at the centerline. Since proppant in the slurry tends to concentrate at the centerline in most fluids, the forward velocity of the proppant is much greater than the volumetric average velocity determined by the flow rate divided by the flow area (Q/A). Figure 1 gives the experimentally determined relative particle velocity determined as a function of sand concentration. In this paper, proppant concentrations are described as volume fraction solids (C_v) which can be easily converted from lb/gallon (p_{pg}) as shown in equation 1 and ρ_g equals the solids density.

$$C_v = \frac{0.1199\,(p_{pg}/\rho_s)}{1 + 0.1199\,(p_{pg}/\rho_s)} \qquad \text{.............} \quad (1)$$

The important fact is, at low concentrations, the proppant moves down the fracture very rapidly compared to the fluid average velocity but slows significantly as the volume fraction of solids increases. Also, as the concentration of suspended solids increases the apparent resistance to flow of the slurry increases. This is in part related to the changing velocity profile across the slot, but it can be interpreted as an increase in apparent viscosity of the slurry.

Figure 2 is a plot of a simplified function describing the observed change in the average (50th percentile) particle velocity (v_p) relative to the volumetric average fluid velocity (v_a) over a range of volumetric particle concentrations. Some degree of experimental data scatter exists because of the relatively small number of observations available. However, the curve shown generally follows the trend of the experimental results. The form of the relation illustrated is shown below:

$$\frac{v_p}{v_a} = 1.27 - Abs(C_v - 0.1)^{1.5} \qquad \text{.............} \quad (2)$$

Apparent Viscosity Increase with Solids Loading: In most fluids, the differential pressure in the fracture increases with increased solids loading. From a numerical simulation standpoint, this is very important since the movement of concentrated slurries will depend totally on the resistance to flow (viscosity). Historically, this seemingly simple measurement has proven to be variable enough that numerous correlations have been published for viscosity versus volume fraction solids. Our own measurements were made with an annular slot viscometer using neutral density beads in a Newtonian fluid and confirmed with subsequent measurements on a Fann Model 50 viscometer.

Differential pressure versus flow rate data were collected at each slurry density. A linear regression analysis was conducted for each data set to determine the relationship between pressure gradient and volumetric flow rate. Results of the regressions were used in conjunction with the geometry of the annular flow cell to calculate the apparent viscosity of each slurry at each flow rate used. Pressure versus rate relations for all cases are very linear indicating no apparent change in rheological behavior with shear rate, even though the velocity profile across the slot changes with solids loading. In addition, the observed differential pressure data were extremely stable at each concentration and flow rate. No long term drift or long equilibration times are apparent in any of the data.

Results of the viscosity calculations resulting from these flow tests are summarized in Figure 3. The plot shows the effective slurry viscosity (μ_a) normalized to the clean fluid viscosity (μ_o) at the same temperature, as a function of volumetric solids concentration (C_v). Data obtained from the annular flow experiments are shown as points. The lines on the plot are derived from several published correlations. The curve defined as BARREE -1.5 is derived from an equation of the form:

$$\frac{\mu_a}{\mu_o} = \left(1 - C_n\right)^{-a} \qquad \text{(3)}$$

where (a) is 1.5 and C_n is the volumetric solids concentration normalized to the maximum attainable solids concentration (C_v/C_{vmax}). Extensive experimentation indicated a maximum packed concentration of 0.64 for the neutral density beads in the Newtonian fluids used in the experiments. With non-Newtonian fluids, different values of (a) and C_{vmax} have been measured. The key point here is that no correlation seems to be universally applicable but the generalized form given in equation 2 where the exponent (a) and C_{vmax} are variables which can be measured experimentally is a reasonable representation of the variations observed. Fluids which have (a) values as low as 1.2 and a C_{vmax} as low as 0.59 show very different slurry flow characteristics. A slurry with these characteristics is much more mobile than the slurry in a Newtonian fluid.

<u>Slurry Settling Correlations:</u> Particle settling rates are typically estimated using Stokes' Law or a similar correlation. The Stokes' equation is limited to a single particle in an infinite fluid mass falling under conditions of laminar flow.

The Stokes' equation is presented for any consistent set of units; for example where v_t is the terminal settling velocity in ft/sec (or cm/sec), ρ is the solid (s) or liquid (l) density in units of lb_m/ft^3 (or g/cm^3), d is the particle diameter in feet (or cm), and μ is the fluid viscosity. Note that a fluid viscosity of 1.0 centipoise is equivalent to 6.72E-04 lb_m/ft-sec (or to 0.01 g/cm-sec). The constant of gravitational acceleration, g, is 32.174 ft/sec^2 (or 980.0 cm/sec^2).

$$v_t = \frac{g(\rho_s - \rho_l)d^2}{18\mu} \qquad \text{(4)}$$

The single particle settling velocities have been modified using a "hindered settling" correlation of the type presented by Govier and Aziz:[27]

$$v_h = v_t e^{-5.9C_v} \qquad \text{(5)}$$

where v_h is the terminal settling velocity of a particle in a slurry with a volumetric solids loading given by C_v. As the solids loading increases the single particle settling velocity in the slurry decreases according to this relation because of particle interactions.

In fracturing operations, slurries are introduced into fractures filled with fluid. Experimentally, slurries were introduced into a vertical slot containing the same fluid without sand. The slurry settling data in Figure 4, shown as open diamonds and squares, indicate that the observed bulk fluid settling velocity exceeds the predicted particle settling rate by more than 100 times at high concentrations. As the solids concentration approaches zero the observed settling rates approach the single particle rate, as expected.

The data also show no significant effect of particle size on observed settling rate. Both the 100 mesh and 30-50 mesh slurries fall at essentially the same rate. Slurry settling rates increase slowly with solids concentration to a maximum at about C_v=0.3. Settling rates remain nearly constant or decrease slightly at higher concentrations as slurry flow resistance increases. At very low concentrations (C_v less than 0.1) the settling rates diverge to the appropriate single particle rates. This suggests that the total observed settling rate is a superposition of the single particle rates and the slurry settling rates caused by bulk density gradients.

The solid line in Figure 4 is the calculated slurry settling rates arrived at by application of Poiseuille's Law for viscous flow between parallel plates. The settling velocity can be estimated assuming that the slurry bulk density variation in the system leads to a fluid potential gradient causing flow. The resulting equation for slurry settling rate (v_s) in feet per second is shown below, where ρ_f is the slurry bulk density (lb_m/ft^3), w is the width of the fracture channel (ft), and μ_a is the apparent viscosity of the slurry (lb_m/ft-sec). Vertical distances relative to an arbitrary datum (h and z) are measured in feet.

$$v_s = -\frac{w^2}{12\mu_a} \frac{\delta(\rho_f \, g \, h)}{\delta z} \quad \text{.............} \quad (6)$$

Note that this equation does not contain the individual particle size. It predicts that the settling rate should increase for denser slurries. However, any increase in slurry viscosity caused by solids addition tends to decrease the settling rate. Adequate use of this formulation therefore requires data of the type presented earlier to describe the increase in apparent viscosity, under representative shear conditions, for the fluid under consideration.

Based on these observations, the transport and settling of proppant slurries appears to be a complex process. Lateral and vertical transport rates are controlled by fluid rheological properties and the local concentration of suspended solids. Individual particle settling occurs concurrently with larger scale convective fluid movements. All these factors must be accounted for in a comprehensive model of proppant transport behavior.

Development of Improved GOHFER Formulation: Marathon's fully three-dimensional hydraulic fracture simulator (GOHFER) incorporates a series of sequential finite difference solutions based on a fixed spatial grid.[24] First the fracture fluid pressures are calculated at each node in the grid by solving an implicit form of the diffusivity equation based on Poiseuille's Law for flow between parallel plates. The pressure solution is then used to determine the fracture width distribution, which is used to iteratively update fluid transmissibilities in the fracture channel. The resulting pressure and transmissibility distributions are then used to calculate local vertical and lateral fluid velocities. The fluid velocity distribution is then used to calculate the concentration distributions of proppant and dissolved components in the fluid stream using an explicit Total Variation Diminishing (TVD) form of the diffusivity equation (such as Equation 7 below).

$$-v \frac{\delta C_v}{\delta x} = \frac{\delta C_v}{\delta t} \qquad \text{.............. (7)}$$

To account for convective proppant movement the fluid pressure distribution (ρ_f) resulting from the diffusivity equation is combined with the slurry bulk density variation throughout the fracture to arrive at the fluid potential distribution. The overall potential gradients, including those caused by density gradients, are used to obtain average fluid velocities by combining Equation 6 with the pressure driven flow terms. The vertical bulk fluid velocity at each node can then be obtained from an equation of the form:

$$v_s = -\frac{w^2}{12\mu_a} \frac{\delta(144P_f\, g_c + \rho_f\, g\, h)}{\delta z} \qquad \text{.............. (8)}$$

Recall that g_c is defined as:

$$g_c = \frac{32.174\ lb_m\ ft}{lb_f\ \sec^2} \qquad \text{.............. (9)}$$

Lateral velocities can be obtained similarly, but the potential gradient caused by density variations disappears for flow parallel to the datum plane.

The resulting fluid velocities are modified by application of Equation 2 to determine a representative particle velocity as a function of proppant concentration. This relation adjusts for the change in velocity profile across the flow channel with changing solids concentration. A different function may be required for each fluid type. The fluid transmissibilities used in the pressure solution are computed using the local apparent slurry viscosity given by Equation 3.

The vertical velocity of the solid components determined from the overall potential field applied to Equation 8 is augmented by the single particle Stokes' settling velocity (given by Equation 4) corrected for hindering using the local concentration (Equation 5). A form of upstream weighing is applied in the TVD formulation to all concentration dependent coefficients.

To correctly model convectively driven transport, relatively sharp concentration fronts must be maintained. The current explicit TVD formulation is capable of maintaining the relatively sharp fronts required. The solution scheme is stable, but requires relatively small node sizes to maintain sharp concentration gradients. For modeling laboratory scale displacements, node sizes on the order of 0.5 ft (0.15 m) square, and timestep sizes of about 0.01 minute give sufficiently sharp fronts. In field scale simulations node sizes of 20' square have been used effectively.

Validation Through Large-Scale Physical Modeling:

The model has been validated by comparison with large scale proppant transport experiments conducted at Stim-Lab, Inc. as part of the Fracturing Fluid Rheology and Proppant Transport Consortium. In these comparisons the diffusive-convective transport model was decoupled from the fracture geometry simulator so that a fixed laboratory flow geometry, with specified boundary conditions, could be modeled.

A series of experiments were conducted at Stim-Lab in the large scale slot flow model using slurries composed of 20/40 mesh sand in 60 lb/Mgal linear HPG gel. These experiments were directed at determining the transport characteristics of various combinations of slurry densities. One such experiment consisted of injecting a 4.0 lb/gal slurry of white sand at a total injection rate of 4 gallons per minute (gpm) followed by a 4.0 lb/gal slurry of the same sand dyed with methylene blue, injected at the same rate.

Results of the numerical simulation of this experiment are shown in Figure 5. The figure consists of contour plots of volumetric solids concentration (C_v) of white sand at four times during the experiment. The fluid flow depicted in the figure is from left to right with an injection rate of 4 gpm. The volumetric solids concentration contour plotted in the figure (C_v=0.10) corresponds to a proppant concentration of about 3 lb/gal.

The top segment in Figure 5 shows the concentration distribution after one minute of injection at a concentration of 4.0 lb/gal as predicted by the numerical transport model. Prior to the start of injection the slot was filled with 60 lb/Mgal HPG flowing at the same rate. The 0.10 concentration contour indicates a slumped proppant distribution with more frontal advance at the slot bottom. The increased lateral transport at the bottom of the slot results from downward convection currents, caused by the density of the injected sand slurry impinging on the slot bottom. With no change in injection concentration this "gravity tongue" continues to develop as the slurry traverses the length of the slot. This is illustrated in the second segment of the figure which represents the predicted concentration distribution after 2.2 minutes of injection with a concentration of 4.0 lb/gal white sand.

The third segment of Figure 5 shows the concentration distribution of white sand after 3.7 minutes of injection consisting of 10.0 gallons of white sand slurry and 4.8 gallons of blue sand slurry, also at 4.0 lb/gal. Note the different character of the concentration contours when the injected blue sand slurry displaces the white sand slurry at the same concentration. No density driven convective settling occurs in the absence of concentration gradients. Instead, the displacement is controlled by the velocity profile established in the slot by injection through only one perforation located one foot from the top edge of the slot.

The velocity controlled displacement, without strong convective action, continues with injection of the 4 lb/gal blue sand slurry. The last segment of Figure 5 shows the white sand concentration contours after 4.9 minutes of injection (10 gallons of white sand slurry and 9.7 gallons of blue sand slurry).

This series of results illustrates that convective settling occurs whenever bulk fluid density gradients exist. No convective settling occurs in the absence of concentration gradients. The slightly skewed concentration gradients shown in segment four result from the induced velocity gradient over the height of the slot. The higher density slurry accumulating near the bottom of the slot due to proppant settling within the slurry itself moves at a substantially lower average velocity than the slurry near the top of the slot. This effect is compounded by the placement of the injection perforation near the top edge of the slot. These strong velocity gradients were clearly observed in the large scale model experiments.

The similarity between the simulator results and the physical experiments is illustrated by Figure 6, which is a composite picture extracted from video tape footage of a Stim-Lab experiment. In Figure 6, the fluid injection point is one foot below the top right corner of the model and flow is right to left. The first vertical support beam to the left of the injection end is four feet from the inlet of the model. The edge of the sand slurry is outlined at two times during the experiment. The sand slurry exhibits a very sharp concentration front, and develops a shallow slope of the stable tongue formed by sand slurry displacing clean 60 lb/Mgal HPG gel.

Application of Results to Fracture Design

One of the most common problems encountered in hydraulic fracturing is a thin productive interval with little if any stress contrast in the non-productive rock above and below the pay zone. A series of stimulation treatment design alternatives were attempted to improve proppant placement. A typical sand shale sequence with low stress contrast was studied. To examine the proppant transport issue with minimum geometry complexities, the tensile strength was set at 800 psi everywhere. Likewise, the Young's modulus and Poisson's ratio were held constant at 4 million psi and 0.25, respectively. Stress was symmetrically varied as shown in Table I. Twenty feet of 0.01 md rock was perforated in the center of the grid with a low leak-off coefficient of 0.001. Thus the condition evaluated here was the stimulation of a low permeability, thin porosity (15%) streak developed in a massive, reasonably uniform formation. The stress was set to 1400 psi in the perforated interval, 1500 psi for the next 40 ft, 1600 psi for the next 60 ft, 1700 psi for the next 60 ft, 1800 for the next 60 ft, and 2000 psi for the next 60 ft symmetrically above and below the pay zone. GOHFER, with its improved proppant transport routines, was used to examine several of the fracture design parameters that are under the control of the design engineer.

The first and most important parameter examined was the common use of a large pad fluid volume. The proposed design is given as Design 1 in Table I. The proppant distribution at the end of pumping and at closure is given in Figures 7 and 8. A minimum amount of proppant was in zone. The major problem with a large pad is the increase in the effects of convective proppant settling by creating a large fracture height into which a dense proppant slurry may fall, especially after shut-in. The job was redesigned with a smaller pad (Design 2) and the proppant distribution at the end of pumping and at closure is given in Figures 9 and 10. Only minor improvements in the proppant distribution were gained, demonstrating that conceptually good ideas still may not achieve the desired goal. A much more aggressive design was examined (Design 3) which still placed the same amount of proppant. The proppant distribution at the end of pumping is shown in Figure 11; at closure is given in Figure 12. The producing zone was still not appropriately propped, compared to the volume of sand pumped. Numerous design options are available. The final design, designated as Design 4, chooses to increase the amount of sand placed in the treatment, but this certainly is not the only approach that could be used. The proppant distribution at the end of pumping and at closure is given in Figures 13 and 14. Even though the amount of sand was increased significantly, 2 lb/ft^2 was only achieved in the producing zone for approximately 200 ft of the fracture. A combination of more sand and increased rate in the later stages was required to achieve the desired result. The higher the rate, the less important convection is in controlling the sand placement. Early in the treatment a low treating rate promotes sand accumulation in the bottom of the fracture near the wellbore. Late in the treatment the higher injection rate forces sand higher in the fracture which settles over the perforations during closure and creates a proppant pack in the producing zone.

The first conclusion from these simulations is that *very* small pads can be used where conventional wisdom has suggested that much larger pads are necessary. Field experience all over the U.S. is continuing to confirm the correctness of this prediction. A second, and more surprising result was the fact that more aggressive sand scheduling does not guarantee a better post-stimulation production result. These conclusions indicate the necessity of examining carefully treatment options before they are implemented to help gain an assurance that the proposed changes in the treatment design will accomplish the desired production result.

Even more confusing is the lack of generalization of this result. Minor changes in the reservoir properties such as tensile strength, Young's modulus and Poisson's Ratio will completely change the predicted fracture geometry and more importantly the effect of the way sand is scheduled in the treatment on the final placement of the proppant after closure. This lack of generalization of the results points out the need to understand the rock mechanics associated with the zone to be stimulated and the variations in the fracture stimulation treatment design that will be required to optimize the stimulation of the well.

Table I: Various Designs Examined for Proposed Stimulation Treatment

Stage	Design 1	Design 2	Design 3	Design 4
Designation	Gallons @ BPM	Gallons @ BPM	Gallons @ BPM	Gallons @ BPM
Pad	20,000 @ 30	2,000 @ 30	1,000 @ 8	1,000 @ 8
2 lb	2,000 @ 30	2,000 @ 30	---	---
3 lb	5,000 @ 30	4,000 @ 30	---	---
4 lb	6,000 @ 30	6,000 @ 30	6,000 @ 8	6,000 @ 8
5 lb	8,000 @ 30	8,000 @ 30	8,000 @ 8	6,000 @ 8
6 lb	10,000 @ 30	10,000 @ 30	10,000 @ 8	8,000 @ 8
7 lb	8,000 @ 30	8,000 @ 30	8,000 @ 8	12,000 @ 12
8 lb	---	---	4,000 @ 8	15,000 @ 15

Conclusions

1. Lateral and vertical proppant transport can be modeled using a combination of single particle and bulk flow mechanics.
2. Proppant transport efficiency of various fracturing fluids can be predicted based on measurable fluid properties.
3. Convective, or density driven, flow occurs whenever fluid bulk density gradients exist.
4. Vertical proppant velocities caused by convective motion can be hundreds of times faster than single particle settling velocities.
5. Proppant placement can be modified by varying injection rate and proppant scheduling.
6. It is very difficult to provide generic designs because the final proppant placement will be affected by many variables including rock modulus and Poisson's ratio, stress, pore pressure, and rock strength.
7. The overall effects of these variables must be integrated into the design parameters that can be controlled such as pad volume, viscosity, pump rate and proppant schedule, using a reliable three-

dimensional fracture simulator which is capable of modeling multi-dimensional fluid and proppant transport with convection. In many cases, the variables affecting slurry flow can be in such a delicate balance that seemingly minor design or reservoir property changes can have a major impact on the production results predicted from the design simulation.

Nomenclature

a	slurry viscosity exponent
A	cross-sectional area
C_n	normalized volume fraction solids
C_v	volume fraction solids
C_{vmax}	maximum attainable solids concentration
d	particle diameter
E	Young's Modulus
g	gravitational constant
g_c	gravitational units conversion constant
h	height above datum
P_f	fracture fluid pressure
P_ϕ	pore fluid pressure
P_{net}	net pressure acting on fracture wall
p_{pg}	proppant concentration, lbs/gal
q	volumetric flow rate
S	distance along fracture surface
v_a	average fluid velocity
v_h	hindered particle settling velocity
v_l	average liquid velocity
v_p	average particle velocity
v_s	slurry transport velocity
v_t	terminal settling velocity
w	fracture width
z	vertical distance
μ_a	apparent slurry viscosity
μ_o	clean fluid apparent viscosity
ν	Poisson's Ratio
ρ_l	liquid density
ρ_f	slurry bulk density
ρ_s	solid density
σ	least principal earth stress
σ_N	net closure stress

Acknowledgements

The authors wish to thank Stim-Lab, Inc., and Marathon Oil Company for permission to publish this paper, and the members of the Stim-Lab, Inc. Rheology and Proppant Transport Consortium for allowing results of the large-scale slot flow experiments to be published. The membership includes:

Acme Resin Corp.
Aqualon Company
BJ Services Company
Carbo Ceramics, Inc.
Chevron Petroleum Technology Co.
Conoco, Inc.
Gas Research Institute
KELCO
Marathon Oil Company
Nowsco Well Service, Ltd.
Pennzoil
Rhone-Poulenc
Shell Development Co.
Texaco E&P Technology Div.
UNOCAL
Weyerhaeuser Company
Amoco Production Company
ARCO
BP Exploration
Canadian FracMaster, Ltd.
China National Petroleum Co.
Schlumberger Dowell
Halliburton Services
Maersk Olie Og Gas as
Mobil E&P Services Co.
ORYX Energy Company
Phillips Petroleum Company
Santos, Ltd.
KSEPL
Union Pacific Resources Co.
Western Co.of North America

The authors would also like to thank Phil Winterfeld for his valuable assistance in incorporating the mathematical formulation of convective proppant transport into the GOHFER simulator and assistance in preparation of this paper.

References

1. Kern, L. R., Perkins, T. K., and Wyant, R. E.: "The Mechanics of Sand Movement in Fracturing," *Trans.* AIME (1959) **216**, 403-405.
2. Babcock, R. E., Prokop, C. L., and Kehle, R. O.: "Distribution of Propping Agents in Vertical Fractures," *Drill. and Prod. Prac.*, API (1967) 207-217.
3. Wahl, H. A.: "Horizontal Fracture Design Based on Propped Fracture Area," *J. Pet. Tech.* (June 1965) 723-731; *Trans.*, AIME, **234**.
4. Lowe, D. K. and Huitt, J. L.: "Propping Agent Transport in Horizontal Fractures," *J. Pet. Tech.* (June 1966) 753-764.
5. Novotny, E. J.: "Proppant Transport," paper SPE 6813 presented at the SPE 52nd Annual Technical Conference and Exhibition, Denver, Oct. 9-12, 1977.
6. Clark, P. E., Harkin, M. W., Wahl, H. A., and Sievert, J. A.:"Design of a Large Vertical Prop Transport Model," paper SPE 6814 presented at the SPE 52nd Annual Technical Conference and Exhibition, Denver, Oct. 9-12, 1977.

7. Hannah, R. R., and Harrington, L. J.: "Measurement of Dynamic Proppant Fall Rates in Fracturing Gels Using a Concentric Cylinder Tester," *J. Pet. Tech.* (May 1981) 909-913.
8. Hannah, R. R., Harrington, L. J., and Williams, D.: "Dynamic Experiments on Proppant Settling in Crosslinked Fracturing Fluids," paper SPE 8342 presented at the SPE 54th Annual Technical Conference and Exhibition, Las Vegas, Sept. 23-26, 1979.
9. Shah, S. N.: "Proppant Settling Correlations for Non-Newtonian Fluids Under Static and Dynamic Conditions," paper SPE 9330 presented at the 55th Annual Technical Conference and Exhibition, Dallas, Sept. 21-24, 1980.
10. Acharya, A.: "Particle Transport in Viscous and Viscoelastic Fracturing Fluids," paper SPE 13170 presented at the 59th Annual technical Conference and Exhibition, Houston, Sept. 16-19, 1984.
11. Kirkby, L. L., and Rockefeller, H. A.: "Proppant Settling Velocities in Nonflowing Slurries," paper SPE/DOE 13096 presented at the SPE/DOE Low Permeability Reservoirs Symposium, Denver, May 19-22, 1985.
12. Sievert, J. A., Wahl, H. A., Clark, P. E., and Harkin, M. W.: "Prop Transport in a Large Vertical Model," paper SPE/DOE 9865 presented at the SPE/DOE Low Permeability Reservoirs Symposium, Denver, May 27-29, 1981.
13. Dunland, A., and Soucemarianadin, A.: "Concentration Effects on the Settling Velocities of Proppant Slurries," paper SPE 14259 presented at the SPE 60th Annual Technical Conference and Exhibition, Las Vegas, Sept. 22-25, 1985.
14. Caswell, B.: "The Effect of Finite Boundaries on the Motion of Particles in Non-Newtonian Fluids," *Chem. Eng. Sci.* (1970) **25**, 167-176.
15. Roodhart, L. P.: "Proppant Settling in Non-Newtonian Fracturing Fluids," paper SPE/DOE 13905 presented at the SPE/DOE Low Permeability Reservoirs Symposium, Denver, May 19-22, 1985.
16. Riddle, M. J., Narvaez, C., and Bird, R. B.: "Interactions Between Two Spheres Falling Along Their Line of Centers in a Viscoelastic Fluid," *J. of Non-Newtonian Fluid Mech.* (1977) **2**, 23-25.
17. Zenz, F. A., and Othmer, D. F.: "The Motion of Single Particles in Fluids," *Fluidization and Fluid-Particle Systems*, Reinhold Publishing Corporation, New York, 227.
18. Joseph, D. D., Nelson, J., Hu., H. H., and Liu, Y. J.: "Competition Between Inertial Pressures and Normal Stresses in the Flow Induced Anisotropy of Solid Particles," *Theoretical and Applied Rheology*, Moldenaers, P. and Keunings, R., eds., Elsevier Science Publishers B. V., Proc. XIth Int. Congr. on Rheology, Brussels, August 17-21, 1992.
19. Leal, L. G.: "The Slow Motion of Slender Rod-Like Paticles in a Second Order Fluid," *J. of Fluid Mechanics* (1975) **69**, 305-337.
20. Clifton, R. J., and Wang, J-J.: "Multiple Fluids, Proppant Transport, and Thermal Effects in Three-Dimensional Simulation of Hydraulic Fracturing," paper SPE 18198 presented at the 63rd Annual Technical Conference and Exhibition, Houston, Oct. 2-5, 1988.
21. Kuenen, P. H.: "Settling Convection and Grain-Size Analysis," *J. of Sedimentary Petrology* (1968) **38**(3), 817-831.
22. Bradley, W. H.: "Vertical Density Currents," *Science* (1965) **150**, 1423-1428.
23. Noh, Y. and Fernando, H. J. S.: "The Motion of a Buoyant Cloud Along an Incline in the Presence of Boundary Mixing," *J. Fluid Mech.* (1992) **235**, 557-577.
24. Barree, R. D.: "A Practical Numerical Simulator for Three-Dimensional Fracture Propagation in

Heterogeneous Media," paper SPE 12273 presented at the SPE Symposium on Reservoir Simulation, San Francisco, Nov. 15-18, 1983.

25. Warpinski, N.R., *et al.*: "Hydraulic Fracture Model Comparison Study: Complete Results," Topical Report No. GRI-93/0109 (February 1993), prepared for the Gas Research Institute under contract no. 5089-211-2059, February1993.

26. Barree, R.D. and Conway, M.W.: "Experimental and Numerical Modeling of Convective Proppant Transport," paper SPE 28564 presented at the 1994 Annual Technical Conference and Exhibition, New Orleans, LA, September 25-28, 1994.

27. Govier, G. W., and Aziz, K.: The Flow of Complex Mixtures in Pipes, Robert E. Krieger Publ. Co., Malabar, FL. (1972) 18.

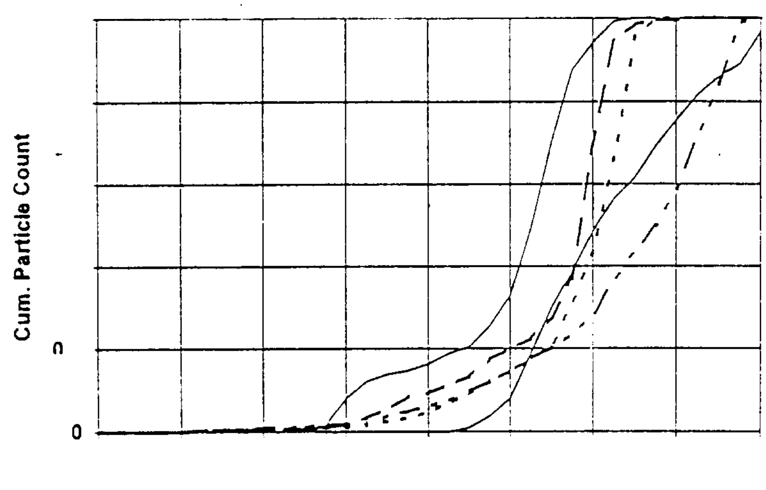

Figure 1 - Particle velocity profiles in annular flow for C_v=0 to 0.55 slurries relative to the bulk average fluid velocity

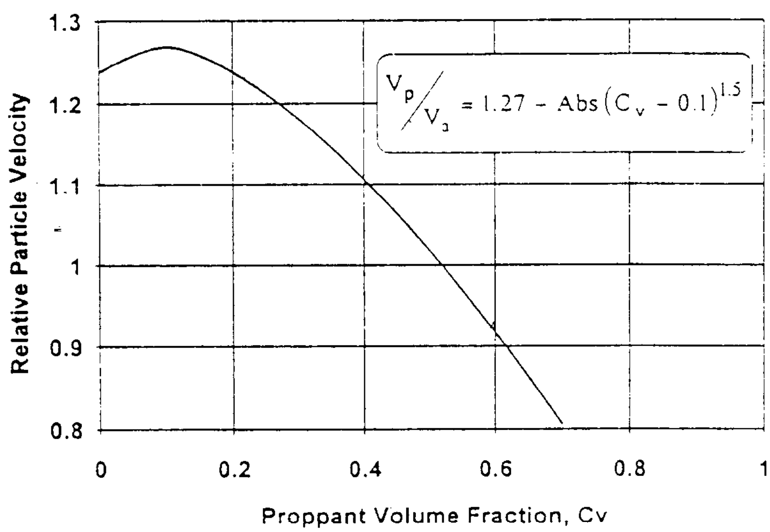

Figure 2 - Simplified relationship for the change in average (50th percentile) particle velocity as a function of volume fraction solids

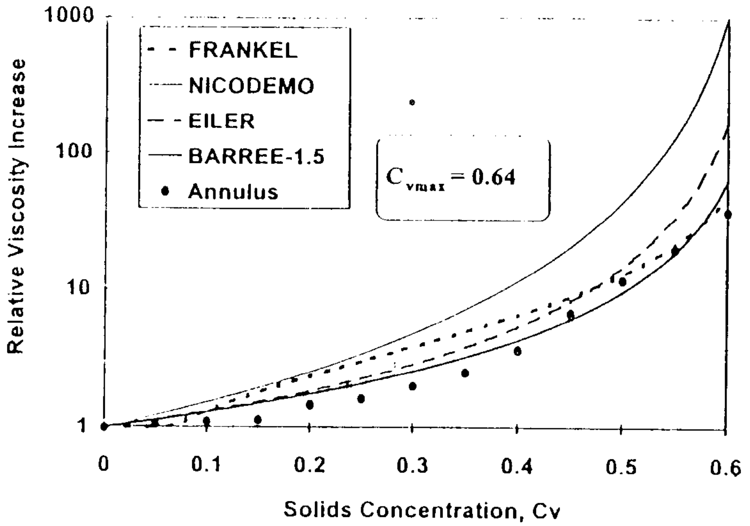

Figure 3 - Apparent solids slurry viscosity from annular flow cell studies at different volume fraction

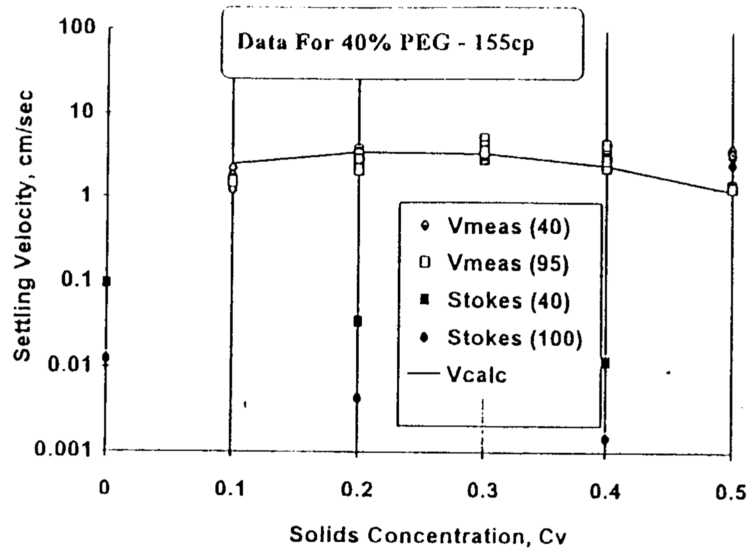

Figure 4 - Observed slurry settling rates in 155 cp Newtonian fluid

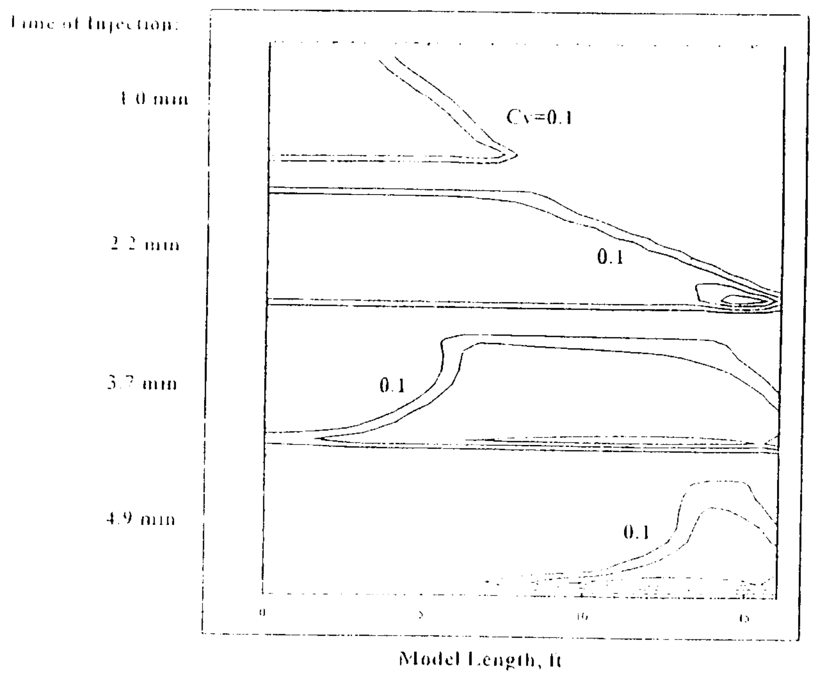

Figure 5 - Calculated proppant volume fraction contours for 4.0 lb/gal slurry in 60 lb/1000 gal HPG in 4 ft high by 16 ft long, 0.31 in wide slot

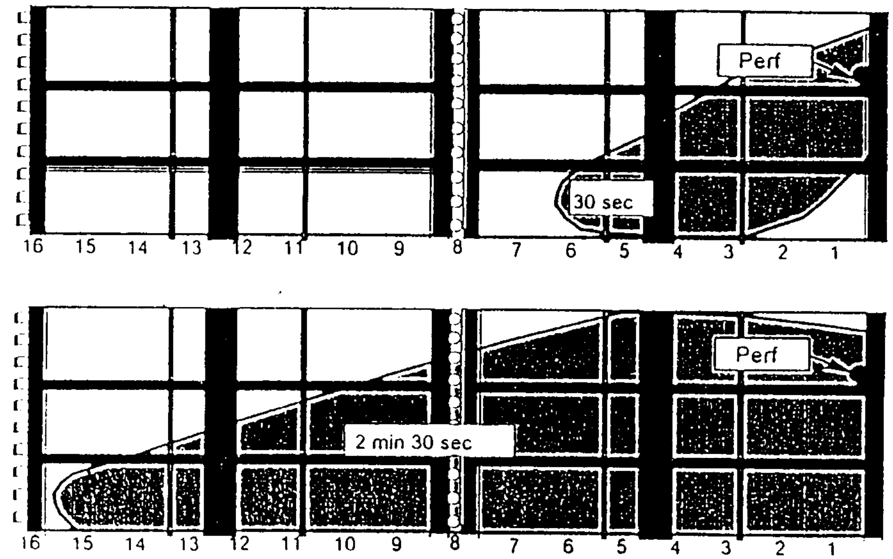

Figure 6 - Slurry distribution in observed large scale physical model experiment with 4 lb/gal sand in 60 lb/1000 gal HPG

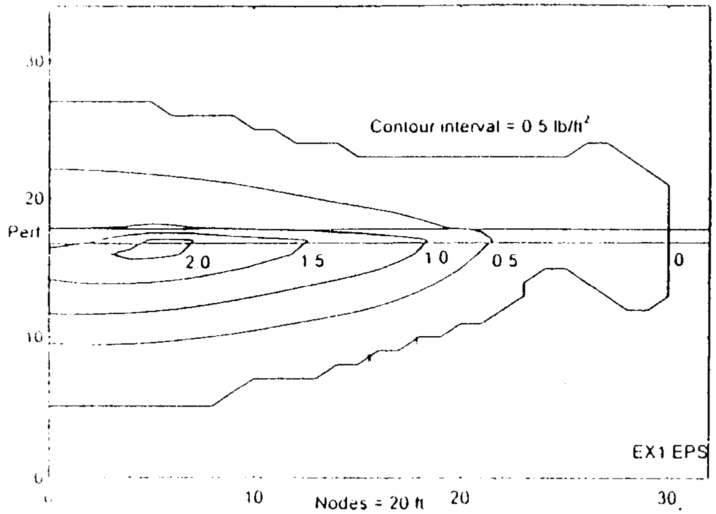

Figure 7 - Proppant distribution for design 1 at the end of pumping

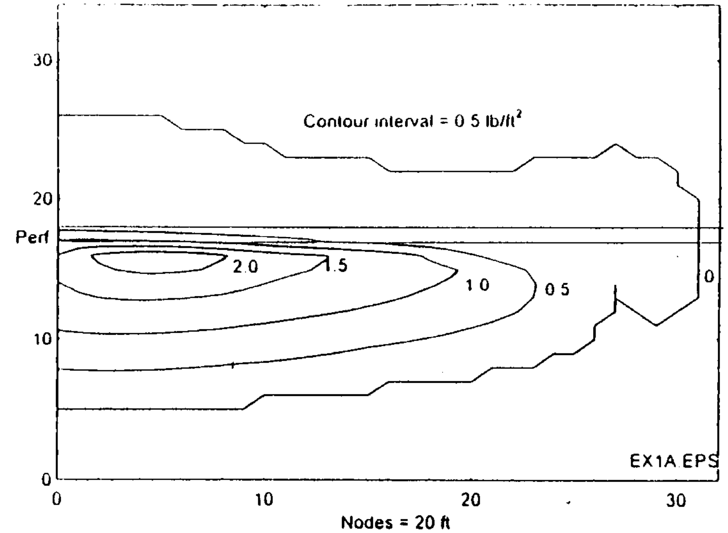

Figure 8 - Proppant distribution for design 1 after closure

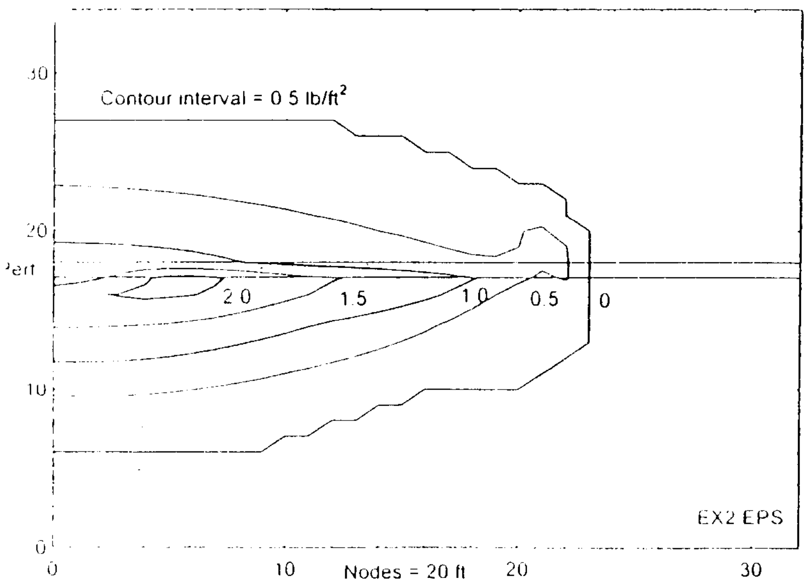

Figure 9 - Proppant distribution for design 2 at the end of pumping

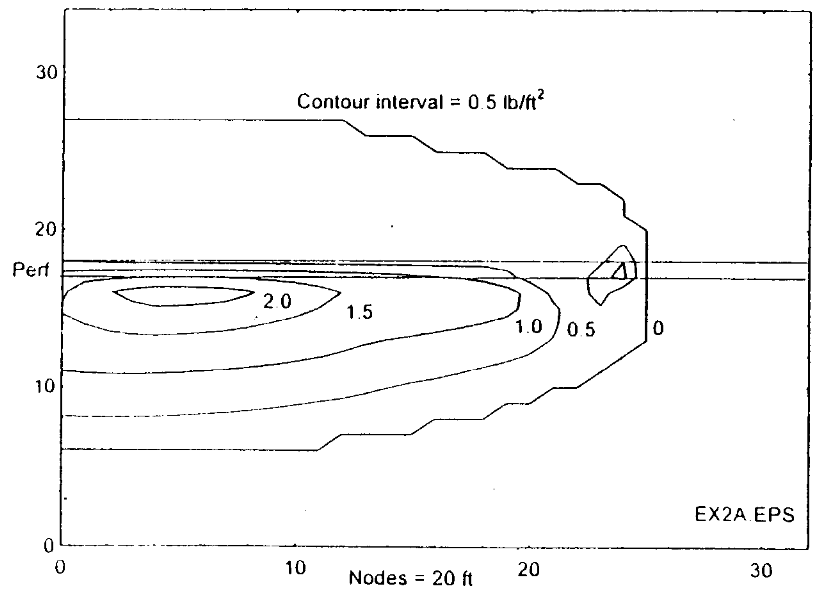

Figure 10 - Proppant distribution for design 2 after closure

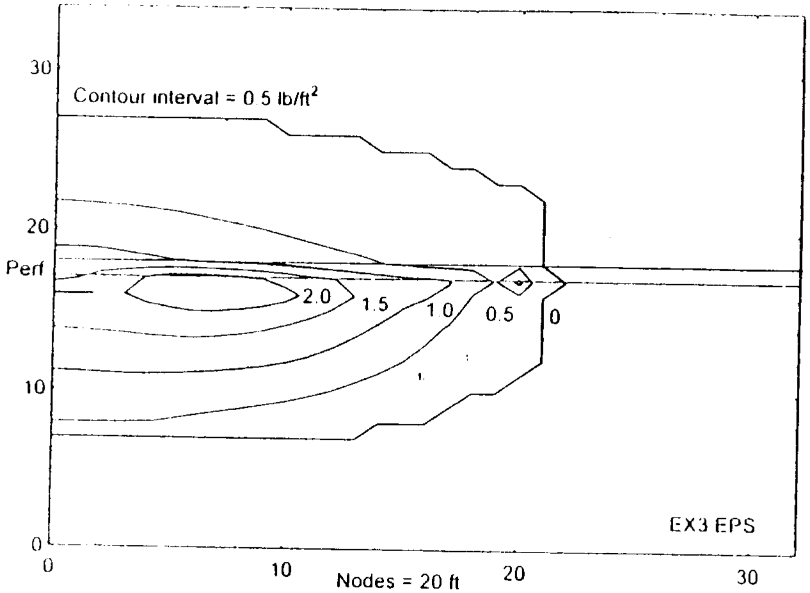

Figure 11 - Proppant distribution for design 3 at the end of pumping

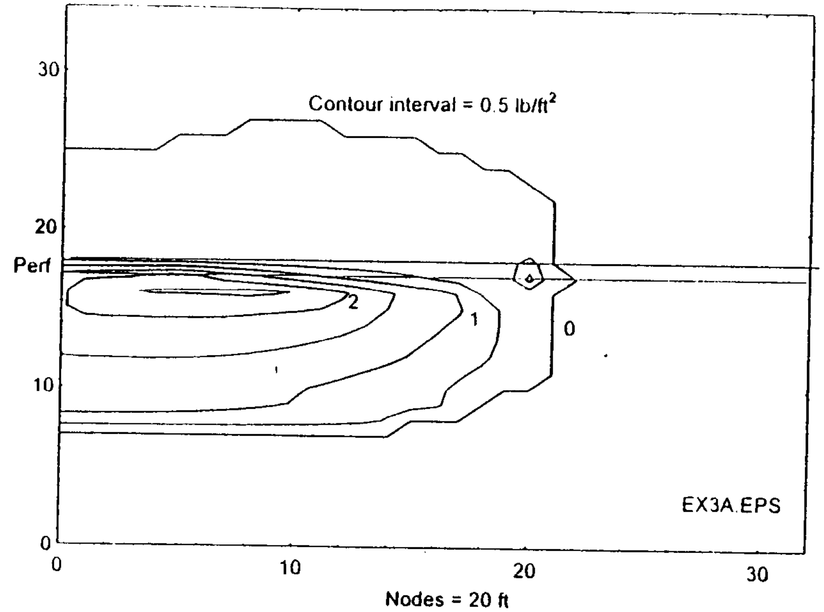

Figure 12 - Proppant distribution for design 3 after closure

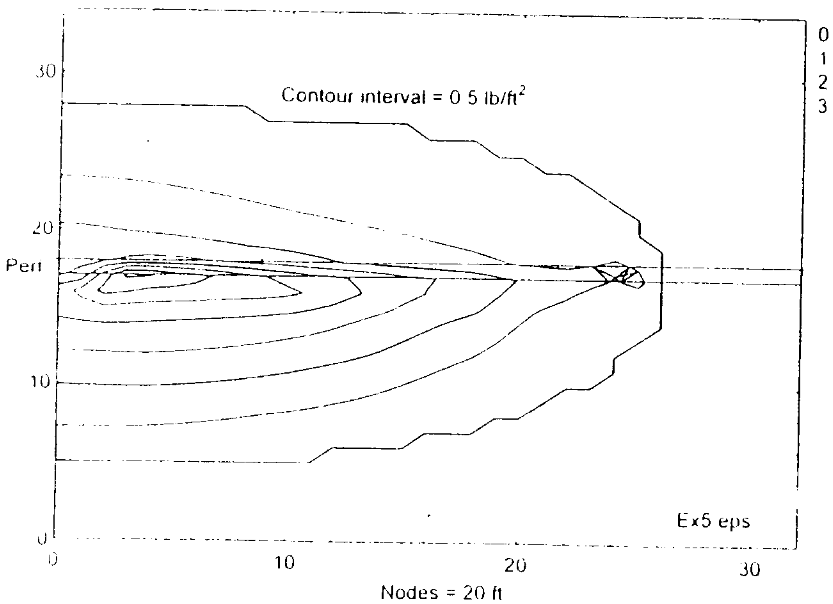

Figure 13 - Proppant distribution for design 4 at the end of pumping

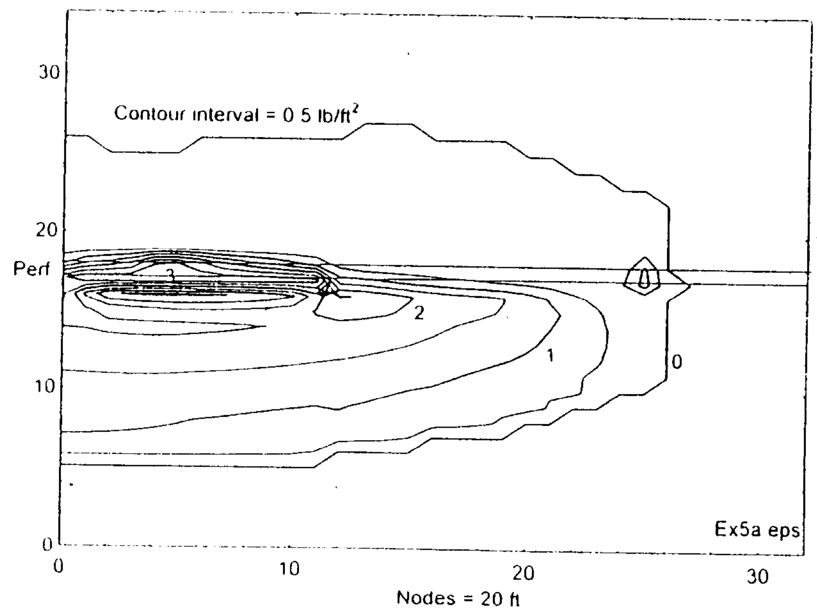

Figure 14 - Proppant distribution for design 4 after closure